dc Magnetoconductivity and Energy Band Structure in Semiconductors

R. M. Broudy and J. D. Venables
National Carbon Research Laboratories, Parma, Ohio*
(Received December 6, 1956)

A general method is described for experimentally obtaining all components of the magnetoresistivity tensor; thence the components of the magnetoconductivity tensor ($\mathfrak{L}$) can be computed. The method is specialized to cubic materials to obtain $\mathfrak{L}(\phi)$, where ϕ is the angle between **H** and the [001] direction in a (100) plane. Mass tensor theory has been developed into a convenient form and applied to this experiment for the three spheroidal cases. Expressions for determination of the mass ratio (K) have been derived. The experiment has been performed on n-type germanium and silicon, verifying the known band structures by means of the angular dependence of $\mathfrak{L}(\phi)$. K has been determined for germanium from 65°K to 200°K.

I. INTRODUCTION

THE usual theories of the behavior of semiconductors under the influence of electric and magnetic fields lead directly to the magnetoconductivity tensor ($\mathfrak{L}$), whereas the usual voltage measurements, due to an applied current, result in the magnetoresistivity tensor ($P=\mathfrak{L}^{-1}$); the Hall constant and magnetoresistance being proportional to two components of P. Comparison of theory and experiment can be made either by mathematical inversion of $\mathfrak{L}$ for comparison with selected components of P or by the much easier arithmetical inversion of P if a suitably designed experiment can be carried out to obtain the independent components. The band structure of n-type germanium and silicon has been determined from dc galvanomagnetic measurements by several investigators[1–5] over the past several years using the former approach; their conclusions have been in close agreement. We shall be concerned here with a method for using the latter approach and in particular with its application to verifying the band structure of n-type germanium and silicon by utilizing the dependence of $\mathfrak{L}$ on the position of **H** in the crystalline lattice. We have reported a preliminary investigation of this approach;[6] its advantages include a more direct correlation between theory and experiment which holds for all **H**—much of the band structure information can be obtained without evaluating the transport integrals. Thus, only very broad restrictions need be made on the form of the relaxation time, τ; on the other hand, knowledge of the transport integrals directly involved in the theory can make possible a more detailed investigation of τ. Similar, although less general, experimental methods have been mentioned by McClure[7] and Juretschke.[8]

II. METHOD FOR MEASURING ALL COMPONENTS OF P

Consider three typical rectangular samples cut from a single crystal, in a Cartesian coordinate system as shown in Fig. 1. **H** can be oriented in any direction.

This arrangement just suffices to obtain all nine components of P. (Only six are independent.) The sample shapes require that for samples A, B and C, the current be in the x, y and z directions, respectively. Thus, the components P_{k1} are measured on A, P_{k2} on B, and P_{k3} on C. For example, P_{11} and P_{21} are measured with the usual resistivity and Hall probes. P_{31} is measured with Hall probes on top and bottom of the sample (or one can turn the sample 90° about the x axis and keep the Hall probes in the usual position—**H** being moved similarly), and the other components follow similarly from samples B and C. One requires only that for any set of components of P, the magnitude and orientation of **H** *with respect to the crystal lattice* remain unchanged.

In most cases, attention to the particular crystal symmetry involved will simplify the experimental difficulties. In addition, it is advantageous to choose the coordinate system in such a manner that the position of **H** can be easily determined and will have significance for the theory; this will usually be such that **H** remains in one of the coordinate system planes which will be chosen as one of the major planes of crystalline symmetry. For cubic materials, which are here considered,

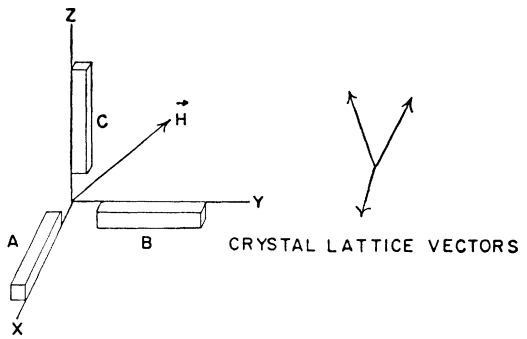

FIG. 1. Experimental arrangement for measuring all components of the magnetoresistivity tensor.

* A Division of Union Carbide and Carbon Corporation.
[1] B. Abeles and M. Meiboom, Phys. Rev. **95**, 31 (1954).
[2] M. Shibuya, Phys. Rev. **95**, 1385 (1954).
[3] W. M. Bullis and W. E. Krag, Phys. Rev. **101**, 580 (1956).
[4] C. Goldberg and R. E. Davis, Phys. Rev. **102**, 1254 (1956).
[5] L. Gold and L. Roth, Phys. Rev. **103**, 61 (1956).
[6] R. M. Broudy and J. D. Venables, Phys. Rev. **103**, 1129 (1956).
[7] J. W. McClure, Bull. Am. Phys. Soc. Ser. II, **1**, 255 (1956).
[8] H. J. Juretschke, Acta Cryst. **8**, 716 (1955).

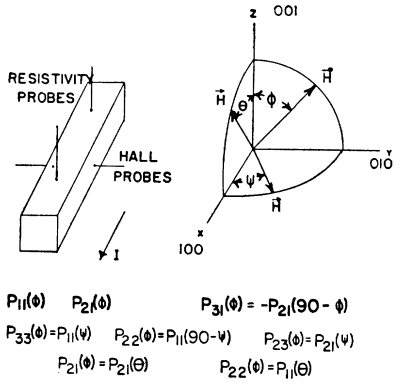

FIG. 2. Experimental arrangement for measuring all components of the magnetoresistivity tensor for a cubic material with **H** in a cubic plane.

we choose the coordinate system to be on axes of cubic symmetry, thus making all three samples equivalent—hence, measurements need be taken on only one sample of this type, as shown by Fig. 2. Thus, we shall obtain $P(\phi)$, where **H** is rotated in a (100) plane at the angle ϕ with respect to an [001] direction. $\mathfrak{L}(\phi)$ is then found by arithmetical inversion of $P(\phi)$.

It should be noted that galvanomagnetic measurements are quite sensitive to inhomogeneities and, in order to obtain valid results, the electrical properties of the material must be essentially uniform over the samples chosen. The presence of nonuniformities will usually be indicated by the deviation of components of $P(\phi)$ from necessary angular symmetry.[9] For example, in a (100) system, $P_{11}(0°)$ must $=P_{11}(90°)$.

III. ANGULAR DEPENDENCE OF $\mathfrak{L}$

In the above-described experiment, the components of $\mathfrak{L}$ must have the following angular dependence for spherical energy bands and isotropic relaxation time (τ): (1) $\mathfrak{L}_{11}(\phi)=C_1$; (2) $\mathfrak{L}_{22}(\phi)=C_1+C_2\sin^2\phi$; (3) $\mathfrak{L}_{33}=C_1+C_2\cos^2\phi$; (4) $\mathfrak{L}_{21}=C_3\cos\phi$; (5) $\mathfrak{L}_{31}=-C_3\times\sin\phi$; (6) $\mathfrak{L}_{23}=C_2\sin\phi\cos\phi$. If the energy band structure and/or τ are not spherical, the components of $\mathfrak{L}$ do not follow these simple angular relations—and it is this deviation which can be used to indicate the type of anisotropy of the material. In this work we investigate the angular variation of $\mathfrak{L}(\phi)$.

IV. GENERAL MASS TENSOR THEORY OF MAGNETOCONDUCTIVITY

The ellipsoidal energy dependence is

$$E=(\hbar^2/2)(k_x^2/m_{xx}+k_y^2/m_{yy}+\cdots+k_xk_y/m_{xy}+\cdots), \quad (1)$$

and components of the reciprocal mass tensor are given by

$$(M^{-1})_{xy}=(1/\hbar)^2(\partial^2E/\partial k_x\partial k_y). \quad (2)$$

[9] We have discovered anomalous magnetoresistance effects in n-type InSb single crystals due to inhomogeneities.

The distribution function for the mass tensor theory was obtained by Bronstein[10] and by Blochinzev and Nordheim[11] in a slightly different form. Making use of both theories, we obtain the current density in the following form:

$$\mathbf{j}=-\frac{e^2}{6\pi^3}\left[(\sum_v \sigma M^{-1})\mathbf{F}+\frac{e}{|M|c}(\sum_v \rho M\mathbf{H})\times\mathbf{F}+\frac{1}{|M|}(e/c)^2(\sum_v \lambda)\mathbf{H}\mathbf{H}\cdot\mathbf{F}\right], \quad (3)$$

where the $\sum_v$'s represent sums over multiple ellipsoids ($\sum_v$ meaning sum over valleys in Herring's terminology), and where

$$\sigma=\int\frac{(\partial f_0/\partial E)\tau(E)Ed\Omega}{1+[e\tau/c]^2(M\mathbf{H}\cdot\mathbf{H}/|M|)},$$
$$\rho=\int\frac{(\partial f_0/\partial E)\tau^2Ed\Omega}{1+[e\tau/c]^2(M\mathbf{H}\cdot\mathbf{H}/|M|)}, \quad (4)$$
$$\lambda=\int\frac{(\partial f_0/\partial E)\tau^3Ed\Omega}{1+[e\tau/c]^2(M\mathbf{H}\cdot\mathbf{H}/|M|)}.$$

The integrals are scalars but depend on the orientation of **H** through the $M\mathbf{H}\cdot\mathbf{H}$ factor.

The integration over $d\Omega$ simplifies to an integration over dE:

$$\int F(E)d\Omega=[4(2\pi)^{\frac{1}{2}}/\hbar^3][m_xm_ym_z]^{\frac{1}{2}}\int F(E)E^{\frac{1}{2}}dE. \quad (5)$$

Thus, for Boltzmann statistics, the integrals are of the form

$$\int e^{-E/kT}\tau E^{5/2}dE,$$

where m_x, m_y, and m_z are the principal axis values of the mass tensor. This can be written as follows:

$$\mathbf{J}\equiv\left[\mathbf{j}\Big/\left(\frac{-e^2}{6\pi^3}\right)\right]=\alpha\mathbf{F}+\mathbf{u}\times\mathbf{F}+d\mathbf{H}\mathbf{H}\cdot\mathbf{F}$$
$$\equiv\beta\mathbf{F}+\mathbf{u}\times\mathbf{F}, \quad (6)$$

where

$$\beta\equiv\alpha+d\mathbf{H}\mathbf{H},$$
$$\alpha=\sum_v \sigma M^{-1}\mathbf{u}=\frac{e}{|M|c}\sum_v \rho M\mathbf{H}\equiv r\sum_v \rho M\mathbf{H}, \quad (7)$$
$$d=\left(\frac{e}{c}\right)^2\left(\frac{1}{|M|}\right)\sum_v \lambda\equiv t\sum_v \lambda.$$

[10] M. Bronstein, Physik. Z Sowjetunion **V2**, 28 (1932).
[11] D. Blochinzev and L. Nordheim, Z. Physik **84**, 168 (1933).

Thus

$$\mathbf{j}=(-e^2/6\pi^3)(\beta+\gamma)\mathbf{F}\equiv\mathfrak{L}\mathbf{F},$$

or

$$\mathbf{J}=(\beta+\gamma)\mathbf{F}\equiv L\mathbf{F}, \tag{8}$$

where β is a symmetric tensor, which is even in $\mathbf{H}$ and γ is an antisymmetric tensor which is odd in $\mathbf{H}$. Equations (6), (7), and (8) determine the method for calculation of L for any multiple ellipsoid energy band system.

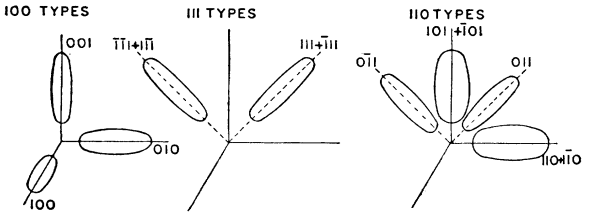

FIG. 3. Effective spheroidal configurations for cubic materials with $\mathbf{H}$ in the (100) plane.

V. MAGNETOCONDUCTIVITY THEORY FOR CUBIC MATERIALS ON CUBIC AXES

We consider here the calculation of components of L for $\mathbf{H}$ in the (100) plane at an angle ϕ with respect to the [001] direction. The effective configurations for the three possible spheroidal arrangements (see, e.g., Shibuya[2]) are shown in Fig. 3.

The 100's remain as shown. The 111's can be considered to coalesce to form a set of two ellipsoids with the three major axes as shown, two on the 45° positions and one in the x direction. The 110's coalesce to form two oblate spheroids (if the original spheroids are considered prolate) with the major axes on y and z directions as shown, the other two prolate spheroids remaining at the 45° positions. The magnetoconductivity components for these three cases are calculated in Appendix A.

The explicit results for L_{11} for the three cases, where in the principal axis system of an 001 spheroid $E=\frac{1}{2}\hbar^2[(k_x^2+k_y^2)/b+k_z^2/a]$, are:

$$L_{11}^A=\left(\frac{1}{b}\right)\int\left(\frac{\partial f_0}{\partial E}\right)\tau E d\Omega\left\{\left(\frac{b}{a}\right)\left(\frac{1}{1+(\omega\tau)^2}\right)+\frac{2+(\omega\tau)^2(1+a/b)}{1+(\omega\tau)^2(1+a/b)+(\omega\tau)^4[(a/b)+\frac{1}{4}(1-a/b)^2(\sin 2\phi)^2]}\right\}, \tag{9}$$

$$L_{11}^B=\tfrac{2}{3}\left(\frac{1}{b}\right)\left(2+\frac{b}{a}\right)\int\left(\frac{\partial f_0}{\partial E}\right)\tau E d\Omega\left\{\frac{2+(\omega\tau)^2(\frac{2}{3})(2+a/b)}{1+(\omega\tau)^2(\frac{2}{3})(2+a/b)+(\omega\tau)^4(\frac{1}{9})[(2+a/b)^2-(1-a/b)^2(\sin 2\phi)^2]}\right\}, \tag{10}$$

$$L_{11}^C=\left(\frac{1}{b}\right)\int\left(\frac{\partial f_0}{\partial E}\right)\tau E d\Omega\left\{\left(1+\frac{b}{a}\right)\left(\frac{2+(\omega\tau)^2(\frac{1}{2})(3+a/b)}{1+(\omega\tau)^2(\frac{1}{2})(3+a/b)+(\omega\tau)^4(\frac{1}{2})[(1+a/b)+\frac{1}{8}(1-a/b)^2(\sin 2\phi)^2]}\right)\right.$$
$$\left.+\frac{2+(\omega\tau)^2(1+a/b)}{1+(\omega\tau)^2(1+a/b)+(\omega\tau)^4(\frac{1}{4})[(1+a/b)^2-(1-a/b)^2(\sin 2\phi)^2]}\right\}, \tag{11}$$

$\omega=(eH)/(ab)^{\frac{1}{2}}c.$

These components are for 3, 4, and 6 spheroids, respectively, and should be multiplied by 2 for 6, 8, and 12 spheroids. As might be expected from observation of Fig. 3, L_{11}^A and L_{11}^B are of the same angular form (except for a constant term) but displaced by 45° and L_{11}^C is of the angular form $C_1L_{11}^A+C_2L_{11}^B$. Thus, the theory determines qualitative criteria for distinguishing among the various possibilities. Although only L_{11} components are shown above, further information can be obtained from other components of L; the method for calculating them follows directly from the appendix. For example, the comparison of relative magnitudes of various components of L serves to determine if $K(\equiv a/b)<1$ or >1.

It is possible to find certain relations among components of L which can determine the value of K from experimental data, once the angular dependence of $L(\phi)$ has determined the correct band structure. We have derived the following relations for determination of K for cases A and B—details are shown in Appendix B.

$$\left[\frac{L_{11}^0-(L_{22}+L_{33})}{K(L_{11}^0-L_{11})-2L_{23}}\right]_{\phi=45^\circ}^A=\frac{1}{2}\left(\frac{K+(1/K)-2}{K(1+K)-2}\right), \tag{12}$$

$$\left[\frac{L_{22}-L_{11}}{L_{11}^0-L_{11}}\right]_{\phi=90^\circ}^B=\frac{9}{(2+K)(2+1/K)}$$
$$=\frac{\rho_0}{\rho_L}\left(\frac{\rho_T^2+(RH)^2-\rho_L\rho_T}{\rho_T^2+(RH)^2-\rho_0\rho_T}\right), \tag{13}$$

where L_{jk}^0 represents the value for $H=0$. These expressions hold for all $|\mathbf{H}|$ and are independent of any assumption on τ except that it be constant on a surface of constant energy. In case B, the symmetrical arrangement of 111 spheroids for this experiment about $\phi=90^\circ$ makes possible a simple relation in terms of components of the magnetoresistivity tensor—K being determined

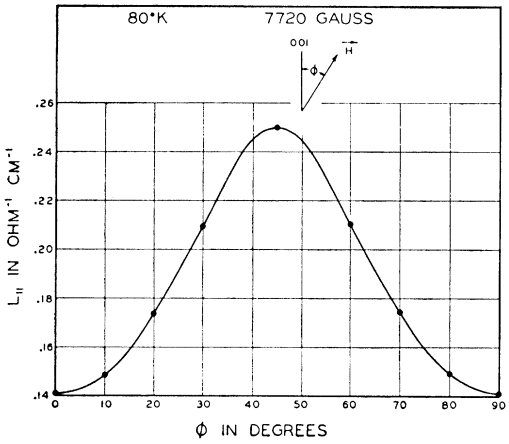

FIG. 4. Transverse magnetoconductivity of n germanium with $\mathbf{H}$ in the (100) plane at the angle ϕ to the [001] direction.

from ρ_L, ρ_T and ρ_0 (longitudinal, transverse, and zero-field resistivity) and R (Hall constant in the appropriate units). RH is essentially the Hall field at the $|\mathbf{H}|$ considered.

VI. EXPERIMENTAL PROCEDURES

Single crystals of n-type silicon and germanium, cut in a 100 system were tested. An ac method of measurements with dc magnetic field is used for speed and elimination of thermal voltages. The sample is mounted on a small brass block separated by a sapphire-insulating plate, probes being mounted from small Teflon terminal blocks attached to the brass. Without removing probes, the brass block assembly can be attached to a copper block inside a Dewar in any of the three mutually perpendicular positions required to measure $P(\phi,\theta,\psi)$ and the whole Dewar is then rotated through 180°, readings being taken with positive and negative magnetic field polarities at each point. Although $P(\phi)$ is needed only from 0–90°, it was necessary to reverse

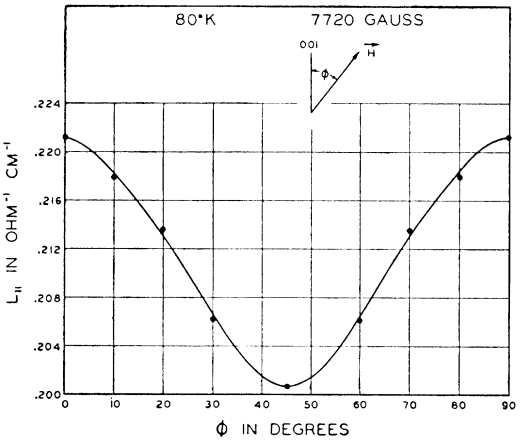

FIG. 5. Transverse magnetoconductivity of n silicon with $\mathbf{H}$ in the (100) plane at the angle ϕ to the [001] direction.

$|\mathbf{H}|$ and take measurements in at least two quadrants in order to eliminate undesired voltages due to probe misalignment.

VII. EXPERIMENTAL RESULTS FOR n-TYPE GERMANIUM AND SILICON

Figures 4 and 5 show $L_{11}(\phi)$ for germanium and silicon. These data are to be compared with (9), (10), and (11). We see immediately that case B applies to germanium and case A to silicon. Case C is ruled out by the single maxima and minima for both curves and by comparison of other components of L. Within experimental error, the angular variation follows exactly that predicted by the integrands of (10) and (9) for Ge and Si; thus τ probably does not vary strongly with energy.

Then using (13) and (12), the apparent mass ratios for Ge and Si at 80°K were computed to be 15.5±0.5 and 5.2±0.5, respectively.

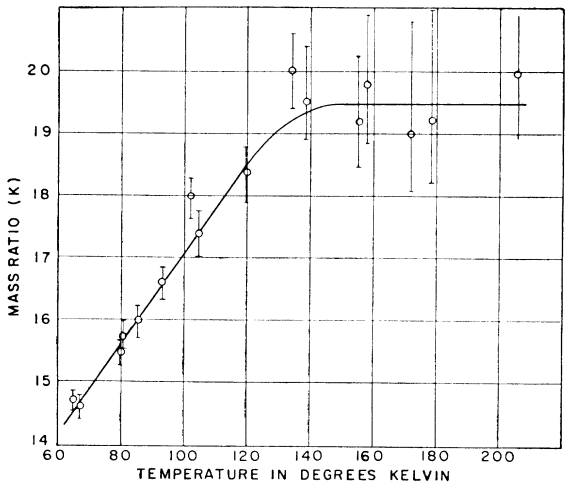

FIG. 6. Apparent mass ratio of n germanium sample as determined from Eq. (13).

Thus, in agreement with the results of others, we can conclude that the energy band structure of germanium consists of 4 (or 8) prolate spheroids with major axes centered along [111] directions and the energy band structure of silicon definitely consists of 3 (or 6) prolate spheroids with major axes centered along [100] directions.

The mass ratio for the germanium sample was determined over the temperature range 65°K to 200°K by measuring ρ_L, ρ_T, and RH; then K was calculated from (13). The results are shown in Fig. 6. Above 130°K the calculated value is close to 20 (the value obtained by cyclotron resonance experiments[12] at 4°K) and decreases rapidly below this temperature. Figure 7 shows a plot of resistivity vs temperature for the same sample over this temperature range; it can be seen that

[12] Dresselhaus, Kip, and Kittel, Phys. Rev. **98**, 368 (1955).

the curve deviates from a $T^{1.69}$ straight line below about 130°K, presumably because of the effects of impurity scattering. This behavior can be interpreted by concluding that the genuine mass ratio does not change appreciably from 4°K to 200°K. Then, if ionized impurity scattering is not isotropic, as predicted by Herring[13] for highly anisotropic energy surfaces, the presence of a relatively appreciable amount of impurity scattering would have an effect on the use of (13). This is so because the derivation of (13) leads back to the original Eq. (3) in which τ is assumed constant over an energy surface. Thus below 130°K, the relatively increasing effect of a nonisotropic scattering would result in a greater departure of the calculated K from its correct value. However, Herring and Vogt[14] have shown that the apparent value of K can correctly be replaced by $K(\tau_\perp/\tau_{\rm II})$ where $(\tau_\perp/\tau_{\rm II})$ is the ratio of

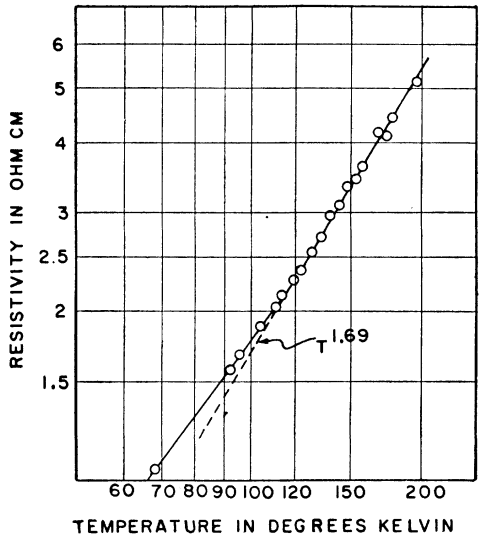

FIG. 7. Resistivity of n germanium sample.

relaxation times in the major axis directions. Thus Fig. 6 actually determines the latter expression; the lattice scattering is probably isotropic.

VIII. CONCLUSIONS

The described technique, subject to the availability of uniform material, can prove a powerful and useful tool for band structure and relaxation time investigation since the close correlation between theory and experiment makes possible more direct information. Although the method has been applied to silicon and germanium in this paper for a particularly chosen orientation of **H**, our purpose has been principally to demonstrate the general significance of the experimental design.

[13] Conyers Herring, Bell System Tech. J. **34**, 284 (1955).
[14] C. Herring and E. Vogt, Phys. Rev. **101**, 944 (1956).

IX. ACKNOWLEDGMENTS

We wish to thank Dr. J. A. Krumhansl and Dr. J. W. McClure for many helpful discussions of this work.

APPENDIX A. CALCULATION OF $L(\phi)$ FOR CUBIC MATERIALS

Figures 8 and 9 show the mass tensors and reciprocal mass tensors for the spheroids of the three cases here considered. The subscripts refer to the direction along which the major axis of the spheroid lies. We calculate the components of L for each spheroid and then sum over the appropriate ones to obtain the terms given by (7) in Eq. (6). **H** is in the yz plane at an angle ϕ with respect to the z axis. We show the details only for the 001 spheroid: from (6), (7), and (8),

$$\mathbf{J}=\begin{bmatrix} \alpha_{11} & -u_3 & +u_2 \\ +u_3 & \alpha_{22}+dH_2^2 & \alpha_{23}+dH_2H_3 \\ -u_2 & \alpha_{23}+dH_2H_3 & \alpha_{33}+dH_3^2 \end{bmatrix}_{001} \mathbf{F}, \quad (14)$$

where α_{ij} and u_k here refer only to the 001 spheroid. Also, from (4) and Fig. 8,

$$\sigma_{001}=\int \frac{(\partial f_0/\partial E)\tau E d\Omega}{1+[\omega\tau]^2[(a/b)\cos^2\phi+\sin^2\phi]}, \quad (15)$$

where

$$\omega=eH/(ab)^{\frac{1}{2}}c,$$

ρ_{001} and λ_{001} being identical except for the replacement of τ by τ^2 and τ^3 respectively. Using Fig. 8, Fig. 9, (7), and (14), we obtain for the components of L due

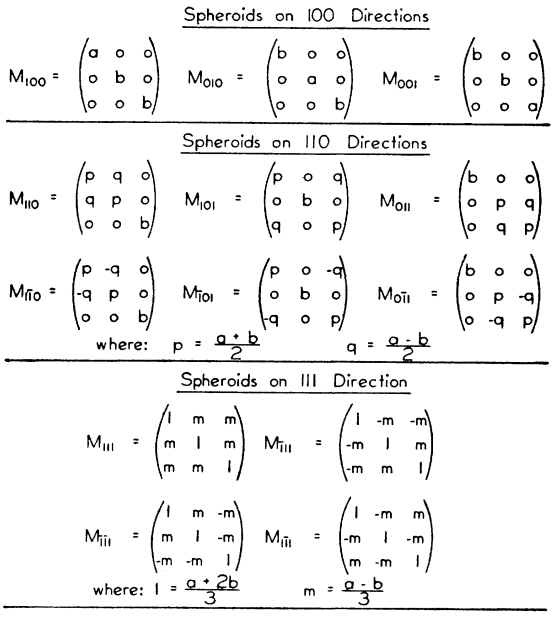

FIG. 8. Mass tensors for the three simplest cubic spheroidal arrangements in a coordinate system on cubic axes. Subscripts refer to major axis directions.

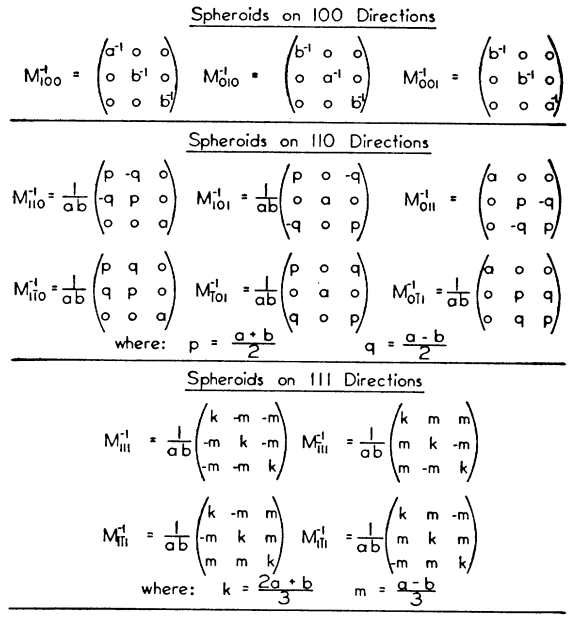

FIG. 9. Reciprocal mass tensors for the three simplest cubic spheroidal arrangements in a coordinate system on cubic axes. Subscripts refer to major axis directions.

to the 001 spheroid:

$$\begin{aligned}
&L_{11}^{001}=\sigma_{001}/b,\\
&L_{22}^{001}=\sigma_{001}/b+tH^2\sin^2\phi\lambda_{001},\\
&L_{33}^{001}=\sigma_{001}/a+tH^2\cos^2\phi\lambda_{001},\\
&L_{23}^{001}=tH^2\cos\phi\sin\phi\lambda_{001}=L_{32}^{001},\\
&L_{21}^{001}=rHa\cos\phi\rho_{001}=-L_{12}^{001},\\
&L_{31}^{001}=-rHb\sin\phi\rho_{001}=-L_{13}^{001}.
\end{aligned}\tag{16}$$

Performing similar computations for 100 and 010 spheroids and adding the total currents, we obtain, using $L^A=L^{001}+L^{010}+L^{100}$:

$$\begin{aligned}
&L_{11}^A=(1/b)(\sigma_{001}+\sigma_{010})+(1/a)\sigma_{100},\\
&L_{23}^A=tH^2\cos\phi\sin\phi(\lambda_{001}+\lambda_{010}+\lambda_{100}),\\
&L_{21}^A=rH\cos\phi[a\rho_{001}+b(\rho_{010}+\rho_{100})],\\
&L_{22}^A=(1/b)(\sigma_{001}+\sigma_{100})+(1/a)(\sigma_{010})\\
&\qquad+tH^2\sin^2\phi(\lambda_{001}+\lambda_{010}+\lambda_{100}),\\
&L_{33}^A=(1/a)(\sigma_{001})+(1/b)(\sigma_{010}+\sigma_{100})\\
&\qquad+tH^2\cos^2\phi(\lambda_{001}+\lambda_{010}+\lambda_{100}),\\
&L_{31}^A=-rH\sin\phi[b(\rho_{001}+\rho_{100})+a\rho_{010}]
\end{aligned}\tag{17}$$

with similar expressions for ρ and λ in τ^2 and τ^3. Similar calculations for cases B and C result in

$$\begin{aligned}
&L_{11}^B=\tfrac{2}{3}(2/b+1/a)(\sigma_{\bar{1}11}+\sigma_{\bar{1}\bar{1}1}),\\
&L_{23}^B=\tfrac{2}{3}\left(\frac{b-a}{ab}\right)(\sigma_{111}-\sigma_{\bar{1}\bar{1}1})\\
&\qquad+tH^2\cos\phi\sin\phi 2(\lambda_{111}+\lambda_{\bar{1}\bar{1}1}),\\
&L_{21}^B=rH(\tfrac{2}{3})[(a+2b)\cos\phi(\rho_{111}+\rho_{\bar{1}\bar{1}1})\\
&\qquad+(b-a)\sin\phi(\rho_{\bar{1}\bar{1}1}-\rho_{111})],\\
&L_{22}^B=\tfrac{2}{3}(2/b+1/a)(\sigma_{111}+\sigma_{\bar{1}\bar{1}1})\\
&\qquad+tH^2\sin^2\phi 2(\lambda_{111}+\lambda_{\bar{1}\bar{1}1}),\\
&L_{33}^B=\tfrac{2}{3}(2/b+1/a)(\sigma_{111}+\sigma_{\bar{1}\bar{1}1})\\
&\qquad+tH^2\cos^2\phi 2(\lambda_{111}+\lambda_{\bar{1}\bar{1}1}),\\
&L_{31}^B=-rH(\tfrac{2}{3})[(a+2b)\sin\phi(\rho_{111}+\rho_{\bar{1}\bar{1}1})\\
&\qquad+(b-a)\cos\phi(\rho_{\bar{1}\bar{1}1}-\rho_{111})],
\end{aligned}\tag{18}$$

$$\begin{aligned}
&L_{11}^C=\left(\frac{a+b}{ab}\right)(\sigma_{110}+\sigma_{101})+\frac{1}{b}(\sigma_{011}+\sigma_{0\bar{1}1}),\\
&L_{22}^C=\left(\frac{a+b}{ab}\right)(\sigma_{110}+\tfrac{1}{2}\sigma_{001})+\frac{2}{b}(\sigma_{101}+\tfrac{1}{2}\sigma_{0\bar{1}1})\\
&\qquad+tH^2\sin^2\phi(2\lambda_{110}+2\lambda_{101}+\lambda_{011}+\lambda_{0\bar{1}1}),\\
&L_{33}^C=\left(\frac{a+b}{ab}\right)(\sigma_{101}+\tfrac{1}{2}\sigma_{011})+\frac{2}{b}(\sigma_{110}+\tfrac{1}{2}\sigma_{0\bar{1}1})\\
&\qquad+tH^2\cos^2\phi(2\lambda_{110}+2\lambda_{101}+\lambda_{011}+\lambda_{0\bar{1}1}),\\
&L_{23}^C=\left(\frac{b-a}{2ab}\right)(\sigma_{011}-\sigma_{0\bar{1}1})\\
&\qquad+tH^2\cos\phi\sin\phi(2\lambda_{110}+2\lambda_{101}+\lambda_{011}+\lambda_{0\bar{1}1}),\\
&L_{21}^C=rH\cos\phi[(a+b)(\rho_{101}+\tfrac{1}{2}\rho_{011}+\tfrac{1}{2}\rho_{0\bar{1}1})+(b)2\rho_{110}]\\
&\qquad+rH\sin\phi\left(\frac{b-a}{2}\right)(\rho_{0\bar{1}1}-\rho_{011}),\\
&L_{31}^C=-rH\sin\phi[(a+b)(\rho_{110}+\tfrac{1}{2}\rho_{011}\\
&\qquad+\tfrac{1}{2}\rho_{0\bar{1}1})+(b)2\rho_{101}].
\end{aligned}\tag{19}$$

TABLE I. The transport integrals are given by

$$\sigma_s=\int(\partial f_0/\partial E)\tau E d\Omega[1+B(\omega\tau)^2]^{-1},$$

with similar expressions in τ^2 and τ^3 for ρ_s and λ_s. B is related to s as shown. $K\equiv a/b$.

s	B
001	$K\cos^2\phi+\sin^2\phi$
010	$\cos^2\phi+K\sin^2\phi$
100	1
111	$\frac{1}{3}(2+K)-2(1-K)\cos\phi\sin\phi$
$\bar{1}\bar{1}1$	$\frac{1}{3}(2+K)+2(1-K)\cos\phi\sin\phi$
110	$\cos^2\phi+\frac{1}{2}(1+K)\sin^2\phi$
101	$\sin^2\phi+\frac{1}{2}(1+K)\cos^2\phi$
011	$\frac{1}{2}(1+K)-(1-K)\cos\phi\sin\phi$
$0\bar{1}1$	$\frac{1}{2}(1+K)+(1-K)\cos\phi\sin\phi$

The transport integrals are given in Table I. The components of L^A, L^B, and L^C can be determined from Table I and (17), (18), and (19) respectively. $L_{11}{}^A$, $L_{11}{}^B$, and $L_{11}{}^C$ are shown in (9), (10), and (11).

APPENDIX B. RELATIONS FOR DETERMINATION OF K

Case B Spheroids.—Using (18), consider the relation

$$[L_{22}{}^B-L_{11}{}^B]_{\phi=90^\circ}=(2\omega^2/b)(\lambda_{111}+\lambda_{\bar{1}\bar{1}1})_{\phi=90^\circ}, \quad (20)$$

and

$$[L_{11}{}^B]_{\phi=90^\circ}=\tfrac{2}{3}(1/b)(2+b/a)(\sigma_{111}+\sigma_{\bar{1}\bar{1}1})_{\phi=90^\circ}. \quad (21)$$

Since all 111-type spheroids are at the same position relative to **H** on an axis of cubic symmetry, the forms of (20) and (21) become simpler. From (18) and Table I, we find

$$[L_{11}{}^B]_{90^\circ}=\left(\frac{4}{b}\right)\left(\frac{2+1/K}{3}\right)\int\left(\frac{\partial f_0}{\partial E}\right)\tau E d\Omega \times\left[1+(\omega\tau)^2\left(\frac{2+K}{3}\right)\right]^{-1}, \quad (22)$$

$$[L_{22}{}^B-L_{11}{}^B]_{90^\circ}=\left(\frac{4}{b}\right)\int\left(\frac{\partial f_0}{\partial E}\right)\tau E d\Omega(\omega\tau)^2 \times\left[1+(\omega\tau)^2\left(\frac{2+K}{3}\right)\right]^{-1}. \quad (23)$$

Now take the relation

$$L_{11H=0}-L_{11\,90^\circ}=\left(\frac{4}{b}\right)\left(\frac{2+1/K}{3}\right)\left(\frac{2+K}{3}\right) \times\int\left(\frac{\partial f_0}{\partial E}\right)\tau E d\Omega[\omega\tau]^2\left[1+(\omega\tau)^2\left(\frac{2+K}{3}\right)\right]^{-1}. \quad (24)$$

Then (23) and (24) lead immediately to (13).

Note that it was not necessary to perform any integrations to obtain (13); thus, this relation has the very general properties of being independent of $|H|$ and of any assumption on τ (other than that of the theory: τ is constant on a surface of constant energy).

Case A Spheroids.—For case A, we find (12) from a similar calculation, using (17) and Table I. This relation also is independent of $|\mathbf{H}|$ and any assumption on τ. The accuracy of the determination of K will increase with $|\mathbf{H}|$, however.

PHYSICAL REVIEW VOLUME 105, NUMBER 6 MARCH 15, 1957

Decay Properties of 74-Second Ag^{111m}†

ULRICH L. SCHINDEWOLF, JOHN W. WINCHESTER,* AND CHARLES D. CORYELL
Department of Chemistry and Laboratory for Nuclear Science, Massachusetts Institute of Technology, Cambridge, Massachusetts

(Received July 23, 1956)

Silver activities were separated by a rapid elution with concentrated HCl from an anion-exchange column containing 22.5-min Pd^{111} as $PdCl_6^=$ from deuteron-bombarded Pd^{110}. The decay of Ag^{111m} was observed with a half-life of 74±3 sec, and its radiations were compared by aluminum absorption with those of 40-sec Ag^{109m}. Conversion electrons and x-rays are seen, with less than 0.1% β decay to Cd^{111}. Search for 49-min Cd^{111m} showed less than 0.01% β decay to this species. Essentially all of the decay of Pd^{111} goes to Ag^{111m}.

INTRODUCTION

IN connection with studies of palladium and silver isotopes found in fission,[1] we have had occasion to consider the isomerism in neutron-rich silver isotopes formed by decay from palladium. The experiments described in this paper are half-life, absorption, and β-spectrometric measurements of short-lived silver activities extracted from deuteron-bombarded palladium in order to characterize Ag^{111m} more sharply.

Short-lived isomeric states are known[2,3] for both of the stable isotopes of silver, 44-sec Ag^{107m} and 40-sec Ag^{109m}. Additional evidence of a short-lived Ag^{111m} has also been reported: its conversion electrons of 60-kev energy have been found[4] in equilibrium with 22.5-min Pd^{111}, an upper limit to its half-life has been set at 5 min,[5] and 48.6-min Cd^{111m2} (11/2) is reported as a decay product.[5]

Because of similarities among Ag^{111}, Ag^{109}, and Ag^{107}, it is not unlikely that Ag^{111m} has a measurably long half-life. In all three, $Z=47$ and N is even. Measured nuclear

† This work was supported in part by the U. S. Atomic Energy Commission.

* Present address: Department of Geology and Geophysics, Massachusetts Institute of Technology, Cambridge, Massachusetts.

[1] J. W. Winchester, Ph.D. thesis in chemistry, Massachusetts Institute of Technology, August, 1955 (unpublished).

[2] R. W. King, Revs. Modern Phys. **26**, 327 (1954).

[3] Hollander, Perlman, and Seaborg, Revs. Modern Phys. **25**, 469 (1953).

[4] C. L. McGinnis, Phys. Rev. **87**, 202 (1952) and private communication cited in reference 3.

[5] P. C. Stevenson and H. G. Hicks (private communication cited in reference 3).